Quantitative Determination of Molecular Chain Tilt Angles in Monolayer Films at the Air/Water Interface: Infrared Reflection/Absorption Spectroscopy of Behenic Acid Methyl Ester

Carol R. Flach, Arne Gericke, and Richard Mendelsohn*

Department of Chemistry, Rutgers University, 73 Warren Street, Newark, New Jersey 07102

Received: July 29, 1996; In Final Form: October 1, 1996[⊗]

Monolayers of behenic acid methyl ester at the air/H_2O and air/D_2O interfaces provide a convenient test for quantitative analysis of infrared reflection−absorption spectroscopy (IRRAS) intensities. Spectra were acquired for both s- and p-polarized radiation at angles of incidence of 35°, 40°, 45°, and 50°. The observed ∼10 cm^{-1} splitting (at a surface pressure of 14 mN/m) for both the methylene scissoring and rocking modes provides direct evidence for the occurrence of a perpendicular orthorhombic subcell structure and for the existence of *all-trans* acyl chains. Analysis of the IRRAS intensities of the methylene and carbonyl stretching vibrations reveals that, of the limited set of chain tilt angles possible with respect to the surface normal, a chain tilt angle of 0° provides by far the best fit to the data. For each vibration, data for both polarizations at all four angles were fit with a single set of three parameters: chain tilt angle, effective extinction coefficient (k_{max}), and the overall degree of polarization (determined by the efficiency of the polarizer and the error in its optical alignment). This last parameter was found to be important in accounting for observed IRRAS intensities, especially for p-polarized radiation close to the Brewster angle. Finally, the feasibility of using the observed unequal intensities in the components of the split methylene scissoring bands to determine the angle that the orthorhombic subcell makes in the *x*,*y* (water surface) plane is demonstrated.

Introduction

In recent years considerable progress has been made in the structural characterization of monolayers at the air/water interface, utilizing techniques such as epifluorescence[1] and Brewster angle microscopy (BAM),[2] X-ray and neutron methods,[3] and infrared reflection−absorption spectroscopy (IRRAS).[4,5] One major goal in the study of monolayers is to determine the orientation of the film-forming molecules. In principle, X-ray and neutron techniques,[6] BAM,[2,7] and IRRAS[8] are all capable of providing this information. BAM has the potential advantage that molecular tilt can be visualized within single domains. However, the accuracy of the tilt angles calculated to date appears limited. In addition to tilt angle information, X-ray and neutron reflection techniques provide the film thickness, the volumes of different interfacial regions, and lattice constants.

A second essential goal in the characterization of monolayers at the air/water interface is the determination of the conformation and structure of the various molecular functional groups. Toward these ends, vibrational spectroscopic techniques are required. Although IRRAS has already provided information about lipid acyl chain conformation and head group hydration as well as the secondary structures of proteins and peptides,[9] the technique has not yet been significantly applied to acquire quantitative information about molecular orientation.

To determine molecular orientation from IRRAS, monolayer films are usually examined using one of two related experimental approaches. The spectral intensities have to be determined either with p-polarization at several angles of incidence or with both s- and p-polarized radiation at a single angle of incidence. Subsequently, an optical model is needed to calculate the orientation of the functional groups giving rise to the IR band. Different mathematical formalisms have recently been compared.[4] Theoretical models yielding similar results were identified. Remaining is the selection of a monolayer system which permits both testing of the optical models and characterization of the experimental setup. In particular, as noted by Gericke et al.,[8] the overall degree of polarization for the experimental setup must be accurately known due to its significant impact on the intensity of bands during studies with "p-polarized" radiation. The monolayer chosen should exhibit the following features: the investigated bands should have a clearly defined transition dipole moment direction with respect to the molecular axis; the molecular tilt angle should be known; and the hydrocarbon chain should exist in the *all-trans* conformation.

We report an IRRAS study of behenic acid methyl ester monolayers, which provide several advantages for testing of optical models. Analysis of the methylene scissoring or rocking modes shows unambiguously that the molecules are organized in a perpendicular orthorhombic subcell. This structure permits only certain chain tilt angles. Quantitative analysis of the methylene and carbonyl stretching vibrations, which exhibit transition dipole moments oriented at 90° with respect to the molecular axis, reveals that the tilt angle is 0°.

Further testing of theoretical models was provided by changing the subphase from H_2O to D_2O. This alters the subphase optical constants and reflectivities and, therefore, the intensities of the observed bands. An excellent fit to the data for both subphases has been achieved with a single set of optical parameters for the film. This provides evidence that the applied optical model and the set of derived optical film parameters is accurate.

The overall degree of polarization for the current experimental setup was established for different spectral regions and is suitable within certain limits for analysis of systems with unknown tilt angles.

* To whom correspondence should be addressed.
[⊗] Abstract published in *Advance ACS Abstracts,* December 1, 1996.

S1089-5647(96)02288-2 CCC: $14.00

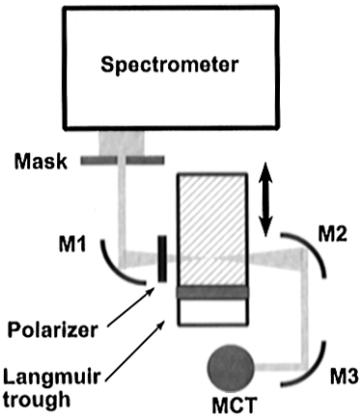

Figure 1. Schematic of the IRRAS setup. M1, M2, and M3 are off-axis parabolic mirrors. M1 and M2 each have focal lengths of 120 mm. MCT = mercury cadmium telluride detector. The arrow indicates the shuttling direction.

Experimental Section

Behenic acid methyl ester (99% purity) was obtained from Sigma (St. Louis, MO) and was used as received. The spreading solvent was chloroform (ACS Certified, Fisher, Springfield, NJ). HPLC grade H_2O water was used (Fisher). D_2O (99.9% isotopic enrichment) was obtained from Isotec (Ohio).

IRRAS measurements were performed on a Biorad FTS 40A (Cambridge, MA) spectrometer equipped with an MCT detector using a home-built optical attachment placed (Figure 1) on a vibration-damped Newport I-2000 table (Fountain Valley, CA). The IR beam is focussed onto the water surface with an off-axis parabolic mirror with a focal length of 120 mm. The angle of incidence was set with an accuracy of $\pm 1°$. A ZnSe wire grid polarizer was obtained from Optometrics (Ayer, MA). The efficiency of the polarizer was specified as ranging from 98.7% (3000 cm^{-1}) to 99.5% (950 cm^{-1}). Throughout the experiment it was possible to alternate between s- and p-polarization. Spectra were acquired with a resolution of 4 cm^{-1} by coaddition of 2048 (s-polarization) or 4096 (p-polarization) scans. Close to the Brewster angle, e.g., for an angle of incidence of 50°, 8192 scans were collected to achieve an acceptable signal-to-noise ratio for p-polarization. One level of zero filling was employed for data presentation.

The thermostatable Langmuir trough was home-built. Surface tension was monitored with a NIMA electrobalance (Coventry, UK). The accuracy of the surface pressure measurement was 0.1 mN/m while the area/molecule was determined to ± 0.005 nm^2/molecule, due to limited accuracy in the determination of the barrier position. Therefore, we refer mainly to surface pressures rather than to areas/molecule. Prior to the spreading, the surface area was reduced and surface active contaminants were suctioned off. An initial clean surface was indicated by zero surface pressures at low trough areas. The temperature was set to 19.0 ± 0.4°C. Humidity in the sample compartment was held constant by an adjustable stream of dry air, resulting in a good water vapor match between reference and sample spectra. The trough was placed on a shuttle device which allows for switching the IR beam between the sample and reference area. The film-forming material was spread at an area of ≈ 0.4 nm^2/molecule, and the film was allowed to relax for at least 45 min prior to compression. The monolayer was compressed discontinuously with an initial step width of 0.008 nm^2/molecule, which was reduced to 0.004 nm^2/molecule in the regions of surface pressures >0 mN/m. After each compression step the monolayer was allowed to relax for at least 5 min. The film was compressed until the surface pressure reached ≈ 17 mN/m, resulting in a total compression time of approximately 3 h. Before data acquisition, the film was allowed to relax for ≈ 1 h, resulting in a decrease of the surface pressure to ≈ 14 mN/m. Throughout the compression no spectra were collected. For each angle of incidence the experiments were reproduced at least four times. IR peak positions were determined with a center of gravity algorithm using software provided by the National Research Council of Canada. All other data manipulations (peak heights and areas, curve fitting) were performed utilizing Grams/32 (Galactic Instruments, Salem, NH).

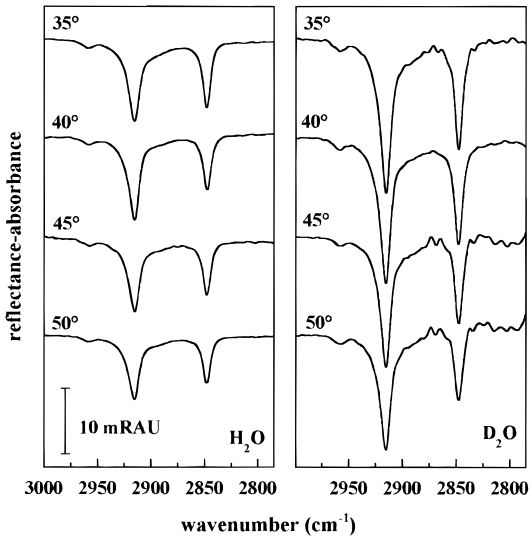

Figure 2. Methylene stretching vibrations for s-polarization of behenic acid methyl ester monolayers ($\Pi \approx 14$ mN/m) on H_2O and D_2O subphases for different angles of incidence. The bar represents an intensity of 10 milli-reflectance−absorbance units (mRAU).

The experimental setup designed for this study offers significant benefits. The use of a shuttle system allows sampling of the film-free surface just prior to acquisition of a monolayer spectrum. This protocol results in the following two advantages. First, a good water vapor match between reference and sample spectrum is achieved. Second, subphase levels in the reference and sample compartments are at the same height. Changes in the subphase level height, observed in the case when longer time periods pass between the acquisition of reference and sample spectra, alter the reflectivity of the system due to changes in e.g., focal lengths. Reflectivity changes caused by such phenomena result in spectral disturbances such as sloping base lines. Another benefit of the described setup is the ability to switch between s- and p-polarized radiation within a single experiment; i.e., the spectra for s- and p-polarized radiation are acquired from the same monolayer, thereby reducing experimental uncertainties.

Results

In Figure 2 the methylene stretching bands of behenic acid methyl ester monolayers for s-polarization on H_2O and D_2O subphases are depicted for several angles of incidence, while in Figure 3 the corresponding spectra for p-polarization are shown. It is found that the bands for D_2O subphases are nearly 2 times stronger than the respective bands for H_2O subphases. In addition, for s-polarization the intensities of the negatively oriented bands decrease with increasing angle of incidence, while for p-polarization the intensity increases and is at a maximum around 45° angle of incidence. The wavenumbers for the asymmetric methylene stretching vibration on H_2O and D_2O are 2915.2 ± 0.1 and 2915.2 ± 0.4 cm^{-1}, respectively.

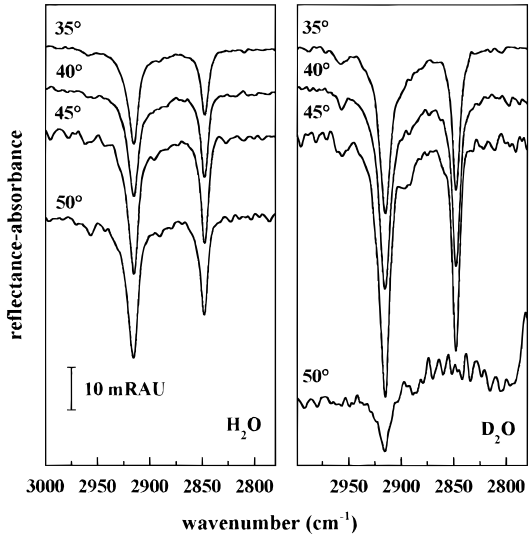

Figure 3. Methylene stretching vibrations for p-polarization of behenic acid methyl ester monolayers ($\Pi \approx 14$ mN/m) on H_2O and D_2O subphases for different angles of incidence. The bar represents an intensity of 10 mRAU.

The reflectivity for H_2O subphases in this spectral region is greater than for D_2O subphases, a possible source of the reduced precision in the frequency measurement in the latter case.

The Brewster angles, determined by calculating the tangents of the real part of the subphase refractive index, are 54.5° and 54.2° for H_2O and 51.1° and 50.7° for D_2O subphases in the spectral region of the asymmetric and symmetric methylene stretching modes, respectively. As shown previously, bands for p-polarized radiation reverse their sign at the Brewster angle.[8] In the spectra for 50° angle of incidence, the intensities of the methylene stretching bands are considerably greater on H_2O than on D_2O for p-polarized radiation to the extent that the symmetric methylene stretching band for p-polarized radiation vanishes with a D_2O subphase. Both these observations are consistent with the difference between the Brewster angle and the 50° angle of incidence for each subphase. As shown later, deviations from ideal polarization characteristics, especially in p-polarized spectra, cause deviations from the expected variation in the intensity with incident angle.

In Figure 4 the spectral region between 1800 and 1400 cm^{-1} is displayed for D_2O subphases and for s- and p-polarization, showing the carbonyl stretching vibration at $\approx$1737 cm^{-1} with a small shoulder at 1720 cm^{-1}, indicating that the majority of the carbonyl groups are unprotonated (in agreement with recent findings by Gericke and Hühnerfuss[10]). The lower frequency shoulder results from protonation of the carbonyl group.[11] The intensities of the carbonyl band decrease with increasing angle of incidence for s-polarization and exhibit an intensity maximum around 45° for p-polarization. However, the quantitative evaluation of the bands at 50° angle of incidence is restricted due to the low signal-to-noise ratio caused by proximity of the angle of incidence to the Brewster angle. The two components of the methylene scissoring bands are observed at 1472.2 and 1462.5 cm^{-1}. This splitting of $\approx$10 cm^{-1} is indicative of a perpendicular orthorhombic subcell[12] and further requires an *all-trans* chain for its detection. The relationship of chain packing and disorder to the magnitude of the splitting of the scissoring bands and to the position of the CH_2 stretching vibrations has been detailed recently.[13] If the frequencies of the asymmetric and symmetric bands (in aqueous phospholipid dispersions) are less than about 2918.8 and 2850.2 cm^{-1}, respectively, any shifts below these values arise from altered packing. Conformational changes are manifest by increases in these wavenumber values by more than a few tenths of a wavenumber. A similar situation is assumed to pertain to the BME monolayers for which the asymmetric CH_2 stretching mode appears at 2915.2 cm^{-1}.

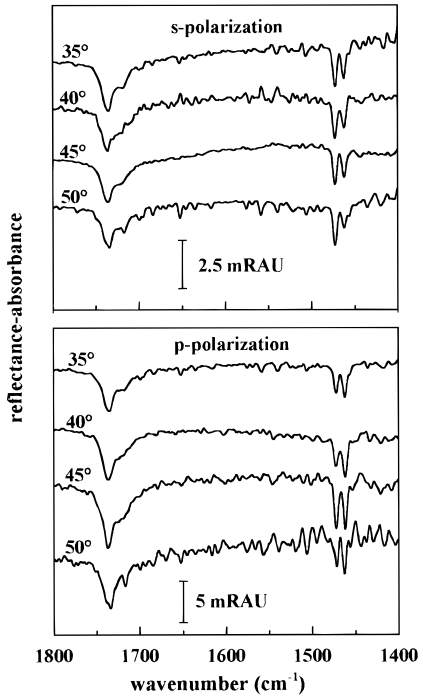

Figure 4. Spectral region 1800−1400 cm^{-1} for behenic acid methyl ester monolayers ($\Pi \approx 14$ mN/m) on D_2O subphases for different angles of incidence. The bar represents an intensity of 2.5 (top) and 5 mRAU (bottom). The band near 1737 cm^{-1} is the C═O stretching vibration, while the split band with components at 1472 and 1463 cm^{-1} is due to the methylene scissoring vibration.

Acquisition of IRRAS at the air/water interface in the 1800−1400 cm^{-1} region is difficult due to the presence of pervasive water vapor bands. Different techniques have been employed to overcome this problem.[11,14] In general, for the s-polarized spectra displayed in Figure 4, the overall residual water vapor band intensity exhibits the same magnitude as the noise level, i.e., the intensity of the water vapor peaks are a fraction of a milli-reflectance absorbance (mRA) unit. To unequivocally assign shoulders such as observed for the carbonyl band, the combined interference from noise and residual vapor bands should be in the range found in Figure 4 for s-polarization at a 45° angle of incidence.

Figure 5 shows the C═O stretching and methylene scissoring bands on an H_2O subphase for p-polarization at 40° angle of incidence. While it is possible to monitor the position of the carbonyl band on H_2O subphases quite accurately, quantitative evaluation of its intensity is complicated by the nearby water bending mode ($\approx$1645 cm^{-1}). The base line exhibits a maximum in this region as a result of dispersion in the water refractive index. Therefore, for the quantitative description of the carbonyl band (see below) the values for D_2O subphases are utilized.

Figure 6 displays the methylene rocking mode on an H_2O subphase at 40° angle of incidence for s- and p-polarized radiation. The split bands are observed at 721.5 and 731.0 $\pm$ 0.5 cm^{-1}. In general, this mode is more difficult to detect from D_2O subphases due to a strong sloping base line (not shown). The comparison of the split methylene scissoring mode for s- and p-polarization (Figure 4) reveals a reversal in the relative intensity of the two components, i.e., for s-polarization the component at $\approx$1472 cm^{-1} is larger than the one at $\approx$1462 cm^{-1},

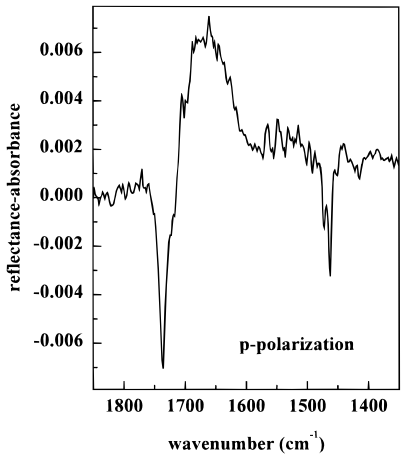

Figure 5. Spectral region 1800−1400 cm^{-1} for behenic acid methyl ester monolayers on an H_2O subphase for p-polarization and 40° angle of incidence. The band near 1737 cm^{-1} represents the C═O stretching vibration, while the split band at 1472 and 1463 cm^{-1} is due to the methylene scissoring vibration.

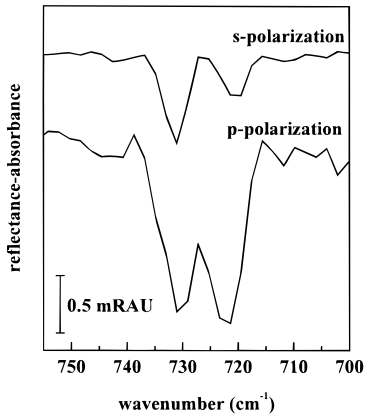

Figure 6. Methylene rocking vibration of behenic acid methyl ester monolayers at 40° angle of incidence on an H_2O subphase. The bar represents an intensity of 0.5 mRAU.

while for p-polarization the opposite is found. The same pattern is found for the methylene rocking mode; i.e., the component which is larger for s-polarization is the smaller one for p-polarization. The origin of the intensity reversal will be addressed in the following section.

Discussion

Optical Model. IRRAS data are reported as plots of reflectance−absorbance (RA) vs wavenumber. RA is defined as $-\log(R/R^F)$, where R is the reflectivity of the film covered surface and R^F is the reflectivity of the film-free surface. RA values can be positive or negative depending on the state of polarization of the incident light, the direction of the change in the dipole moment during the normal mode, and the magnitude of the incident angle relative to the Brewster angle. Various optical models have been employed to describe IRRAS band intensities. These were recently compared by Mendelsohn et al.[4] Three formulations (Schopper,[15] Kuzmin and Michailov,[16] and Yamamato and Ishida[17]) that start from quite different premises produce similar results upon computer simulation. We select one of these methods, the mathematical formalism developed by Kuzmin and Michailov,[16] which was first applied by Gericke et al.[8] to describe IRRAS band intensities. The formulas are given in Appendix A.

The following parameters are required to calculate a reflectance−absorbance value using the aforementioned mathematical

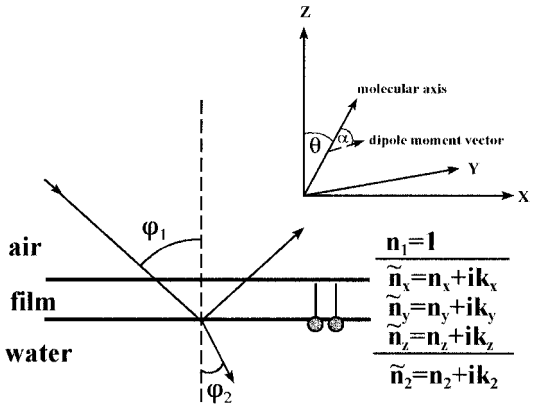

Figure 7. Optical constants for the three-phase system: air, homogeneous, anisotropic monolayer, and isotropic liquid substrate, and the axis system used for describing IRRAS geometries. Symbols are described in the text.

TABLE 1: Parameters Needed for the Calculation of Reflectance−Absorbances of Monolayers at the Air/Water Interface

quantity	origin of numerical value
φ_1	experimental setting
λ	convert wavenumber to wavelength
n_1, k_1	$n_1 = 1$; $k_1 = 0$ (air)
n_2, k_2	given in ref 28; interpolated to the desired stepwidth
α	90° for the vibrations discussed in this paper
n	$\nu_a(CH_2)$ and $\nu_s(CH_2)$, 1.41 ± 0.01;[18] ν(C═O), 1.40 ± 0.01[19]
L	X-ray, molecular modeling or Tanford[20]
k_{max}	computer simulation
θ	normally computer simulation, herein shown to be 0°, primarily from the presence of the $\delta(CH_2)$ splitting
Γ	computer simulation

formalism (see Figure 7 for depictions of the various coordinates): angle of incidence, φ_1; mean tilt angle of the molecular axis relative to the surface normal, θ; the angle that the transition dipole makes with the molecular axis, α; vacuum wavelength of the light, λ; monolayer thickness, d, which can be obtained by taking into account the tilt angle for a molecule of known length L; the degree of polarization of the optical setup, Γ; indices of refraction and extinction coefficients of the incident and final phases, n_1, n_2, k_1, k_2; and the directional refractive indices and extinction coefficients of the monolayer, n_x,n_y, n_z, k_x, k_y, k_z. Table 1 summarizes how these values are obtained.

The real part, n, of the film refractive index can easily be separated into its directional components n_x, n_y, and n_z (see, e.g., ref 4). However, results from computer simulation revealed that minor changes in the real part of the film refractive index (±0.02) do not alter the obtained reflectance−absorbances significantly. Therefore, the isotropic values are used throughout the paper. In the literature,[8] values of ≈1.5 are frequently used for the refractive index of the methylene stretching vibrations, which is the value found for hydrocarbons in the visible region of the spectrum. However, exact analysis by IR ellipsometry showed that these values are too high. Values of 1.41 ± 0.01 should be used both $\nu_a(CH_2)$ and $\nu_s(CH_2)$.[18] Similarly, the value for ν(C═O) was found[19] to be 1.40 ± 0.01.

Using Fraser and MacRae's[21] formalism (Appendix B), the directional extinction coefficients $k_x = k_y$ and k_z can be obtained for a given tilt angle and transition moment direction when k_{max}, the film extinction coefficient, is known. The magnitude of k_{max} depends on the strength of the oscillator and the density of the film forming molecules at the air/water interface. Therefore, k_{max} will vary throughout the compression of the monolayer. As a result, three parameters which are required to calculate

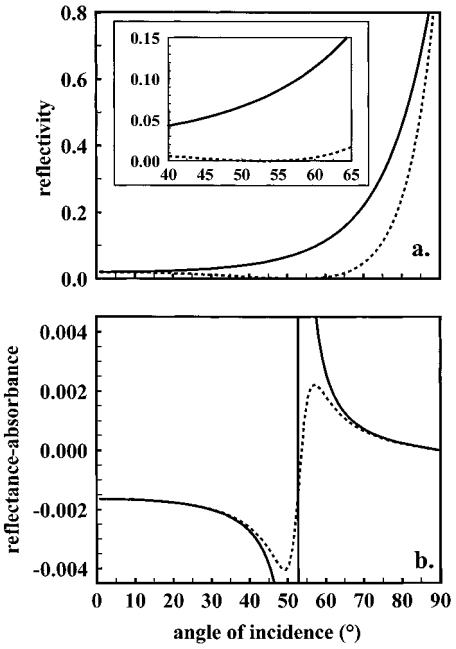

Figure 8. (a) Reflectivity curves: R_s (s-polarization, —) and R_p (p-polarization, - - -) vs angle of incidence for a pure water surface. (b) Reflectance−absorbances vs angle of incidence for p-polarization for an ideal polarizer (—) and for a polarizer with 98.8% degree of polarization (- - -).

reflectance−absorbances are normally unknown: k_{max}, the tilt angle, θ, and the degree of polarization, Γ.

For the experiments described here, the tilt angle of the molecule is most likely 0° for the following reasons. The observed splitting of the $\delta(CH_2)$ band indicates a subcell which is orthorhombic perpendicular. This can exist in either an orthorhombic (0° tilt angle) or a monoclinic (≈30° tilt angle) space group. Both discrete chain tilt angles allow for the intermolecular coupling necessary for the full splitting of the scissoring mode, although at ≈30° the methylene groups in adjacent chains are offset by one carbon atom from each other.[12,22] The molecular area requirements in the plane of the monolayer vary for the two tilt angles, where a greater area is required for a larger tilt. First, under the conditions of the current experiment, the molecular area available for the behenic acid methyl ester molecules is close to that occupied for a 0° tilt.[23] Second, recent findings by BAM for behenic acid methyl ester monolayers above the kink point in the pressure/area isotherm also indicate a tilt angle of zero.[24] Third, simulations of IRRAS band intensities calculated using a chain tilt of ≈30° do not agree with the observed IRRAS results, whereas the simulations performed using an acyl chain tilt of 0° are in close agreement with the measured data (see below).

An important factor, neglected in most quantitative IRRAS studies to date, is the degree of polarization of the optical setup. The degree of polarization for good polarizers is usually specified as between ≈98.5 and 99.5% in the 3000−1000 cm^{-1} spectral region. As a result of experimental inaccuracies, e.g., the setting of the polarizer, the actual degree of polarization may be even less. In Figure 8a the reflectivity curves R_s and R_p for s- and p-polarization are displayed. It is found that the reflectivity for s-polarization is higher than for p-polarization at all angles of incidence. This is particularly pronounced near the Brewster angle. In Figure 8b the reflectance−absorbances for p-polarized (RA_p) light are displayed for an ideal polarizer and for a polarizer with 98.8% polarization. The observed intensity increase in the ideal RA_p curve upon approaching the Brewster angle is due to the diminution of the reflectivity of the film-free water surface R_p^F, which corresponds to an increase in the magnitude of the reflectance−absorbance ($-\log(R_p/R_p^F)$). However, a small portion of s-polarized radiation "leaking" through the polarizer will lead to larger reflectivities from film-free surfaces. The observed reflectance−absorbance will be smaller than predicted for pure p-polarized radiation (see Figure 3 for D_2O subphase data at 50° angle of incidence). To account for nonideal polarization effects, the following formula was applied by Gericke et al.[8] to calculate the effective reflectivities for the film-free and film-covered surfaces.

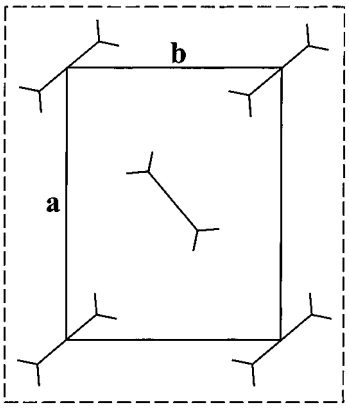

Figure 9. Orthorhombic subcell structure for hydrocarbon chains.

$$R_p^{eff} = R_p + \Gamma(R_s - R_p)$$

where R_p and R_s are the ideal reflectivities for p- and s-polarization, respectively, while $\Gamma = I_s/I$. (I_s is the s-polarized intensity, and I is the total intensity of light passing through the polarizer when set to p-polarization.) Subsequently, these effective reflectivities are used to calculate RA values. The data presented in Figure 8b show that even for incident angles removed by as much as 10° from the Brewster angle, the influence of s-polarized light cannot be neglected. At an angle of incidence of 40°, the difference between the "ideal" and "nonideal" reflectance−absorbance values is 5.2%, and at 75°, the difference is 7.5%. This effect may explain the discrepancy between calculated and measured values found by various authors (Fina and Tung,[8] Ren et al.[8]). In contrast, reflectance−absorbances for s-polarized radiation are practically undisturbed by p-polarized radiation leaking through the polarizer. In principle, it is possible to evaluate the degree of polarization for a *known* tilt angle simply by comparing measured and calculated reflectance−absorbances at a single angle of incidence for p- and s-polarization. For greater accuracy, we recommend measuring p- and s-polarized RA's for a variety of angles of incidence. It is not possible to determine the degree of polarization for an unknown tilt angle at a single angle of incidence because the problem is mathematically underdetermined. (There are three unknowns—k_{max}, Γ, and the tilt angle—with only two observable intensities.) In the following section, a computer simulation is used to obtain the combination of k_{max} and Γ which best fits the measured RA's at several angles of incidence.

The mathematical formalism as outlined in the appendices assumes a uniaxial system with free rotation around the molecular axis. However, for an orthorhombic subcell structure (Figure 9) the condition of free rotation around the molecular axis is clearly not fullfilled, i.e., the molecules are oriented in the *x,y* plane. In principle, it is possible to account for this by including a chain orientation angle for the *x,y* plane in the mathematical formalism,[8,25] resulting in $k_x \neq k_y$. However, due

to the orthogonality of the two molecules in an orthorhombic subcell, for IR bands where splitting by intermolecular coupling cannot be detected, the resulting k_x must be equal to k_y for any orientation of the subcell in the x,y plane. In particular, this holds for bands such as the methylene or carbonyl stretching modes. As will be shown later, the intensity of the components of modes split due to intermolecular interaction are indeed affected by the nonrandom orientations of the subcell in the x,y plane.

Comparison of Measured and Calculated Reflectance−Absorbances. The intensities of the measured bands were obtained by evaluation of the peak heights after the bands were base line corrected. The advantage of using the peak heights rather than the integrated intensites is that the results are less dependent on interference from adjacent, partially overlapped spectral features.

To simulate the reflectance−absorbances, the following procedure was employed. The whole band contour was simulated assuming a Lorentzian band shape using the full width of the band found experimentally (see Appendix B). The side lobes of the simulated negatively oriented band are above zero, which is caused by the dominance of the real part of the monolayer refractive index over the imaginary part in this region. Furthermore, the distribution of intensity is unequal between the two side lobes due to the anomalous dispersion in the refractive indices of the monolayer and subphase. Therefore, the simulated band needs to be base line corrected to obtain its total intensity. Peak positions are shifted from those measured in transmission experiments. It is possible to account for this by Kramers−Kronig analysis (Yamamoto and Ishida[26]). In the current work, we simply varied the input center frequency used for the calculation of the Lorentzian band shape (Appendix B) to yield the measured band positions, and the intensities were determined at this frequency. To find the best fit to the experimental values, a set of data were calculated by using different combinations of k_{max} and Γ values. The best combination was determined by comparing the sum of the squares of the difference between measured and calculated RA's for all the different incident angles as measured with both p- and s-polarized radiation.

Results of the Simulation. In Figure 10 the results for the simulated peak intensities of $\nu_a(CH_2)$ are compared to the measured ones for D_2O and H_2O subphases. In general, the intensities are radically different for the two subphases, which is a result of the different subphase refractive indices. For all data sets the same parameters were used, i.e., $k_{max} = 1.07$ and $\Gamma = 0.014$. The quality of the fit convincingly demonstrates the validity of the optical formalism applied. In general, information about the anisotropy of the monolayer, i.e., about molecular orientation, can best be obtained in the vicinity of the Brewster angle.[8] The Brewster angle for D_2O at 2916 cm^{-1} is 51.1°, while for H_2O the value is 54.5°. (In Figure 10, the calculated curves are based on nonideal polarization; the "apparent" Brewster angles in this figure therefore differ slightly from those noted above.) One experimental problem that arises near the Brewster angle for p-polarized radiation is an increase in the noise due to the low reflectivity. Another problem is that a minor error in the setting of the angle of incidence causes strong changes in the reflectance−absorbance. This can be seen (Figure 10) when the measured and calculated RA_p values for the D_2O subphases are compared. The value measured for a 50° angle of incidence is shifted ≈1° with respect to the calculated curve. However, the comparison of the intensities at exactly 50° shows that the measured value is approximately 50% of the calculated value. Considering this and taking into account the strong influence of the degree of polarization on the measured reflectance−absorbances, it is not advisable to rely on quantitative analysis where data are acquired too close to the Brewster angle. In general, results similar to those for the asymmetric CH_2 stretching modes are found for the symmetric CH_2 stretching modes (data not shown).

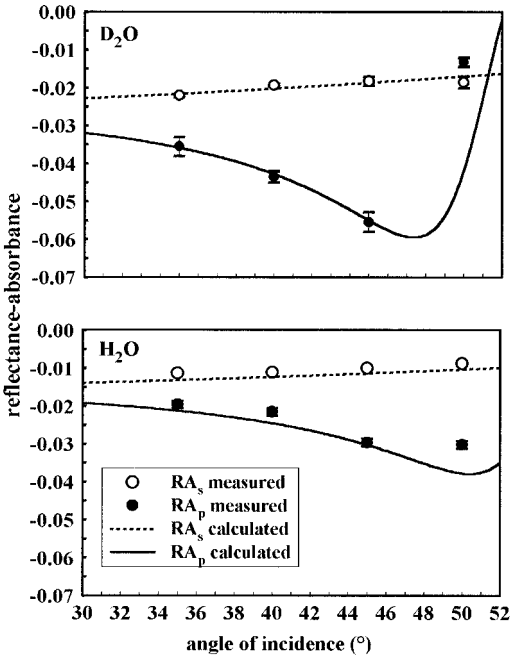

Figure 10. Comparison of the simulated (solid and dashed lines for p- and s-polarization respectively) and measured (solid and open circles for p- and s-polarization, respectively) peak intensities for $\nu_a(CH_2)$ on D_2O (top) and H_2O (bottom) subphases, respectively. The surface film parameters for the simulation were $k_{max} = 1.07$, $n = 1.41$, $\Gamma = 0.014$, tilt angle = 0°; $d = 3.06$ nm, and $\alpha = 90°$.

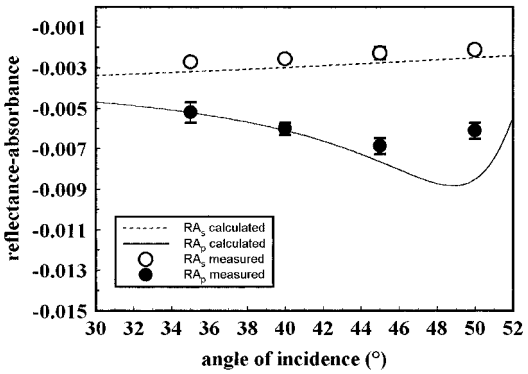

Figure 11. Comparison of the simulated and measured peak intensities for the carbonyl stretching vibration on a D_2O subphase. Symbols and lines as in Figure 10. The surface film parameters for the simulation were $k_{max} = 0.38$, $n = 1.40$, $\Gamma = 0.013$, tilt angle = 0°, $d = 3.06$ nm, and $\alpha = 90°$.

In Figure 11 the measured intensities for the carbonyl stretching band are compared to the simulated ones. The Brewster angle at 1738 cm^{-1} is ≈53.1°. The best fit was obtained for $\Gamma = 0.014$ and $k_{max} = 0.38$. The values for p-polarization at a 50° angle of incidence are not very well matched, but it should be noted that the accuracy of the measured peak height is limited for this particular angle of incidence because of the reduced signal-to-noise ratio (see Figure 4).

Orientation of the Molecules in the *x,y* Plane. Generally, an orthorhombic subcell can be arranged at any angle in the x,y plane. It is likely that this orientation will change from one experiment to the next. The most convenient way to determine

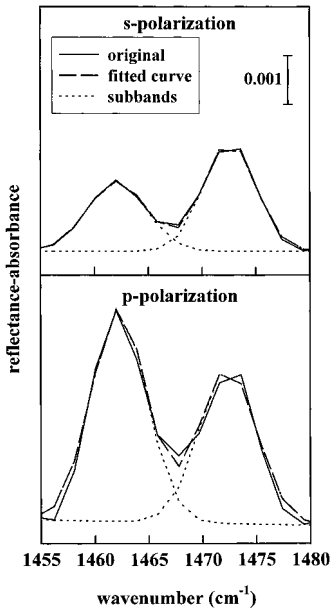

Figure 12. Comparison of the split methylene scissors mode for s- and p-polarization (top and bottom, respectively). The solid line represents the original spectra and dotted lines the subbands, while the long dashed line is the sum of the fitted components as obtained by assuming a Gaussian band shape. The bar represents 1 milli-reflectance−absorbance unit.

this orientation is to quantitatively analyze the splitting of the methylene scissoring mode. As previously mentioned, the magnitude of the splitting of this band indicates a perpendicular orthorhombic structure. The splitting is caused by intermolecular interaction between adjacent molecules in the orthorhombic subcell. Snyder[27] has shown that the higher frequency component ($\approx$1472 cm^{-1}) of the split orthorhombic $\delta(CH_2)$ mode is polarized in the "*a*" direction of the subcell (see Figure 9). In turn, the lower frequency component ($\approx$1462 cm^{-1}) represents the part of the transition moment which is polarized along the "*b*" axis of the subcell. The same holds for the rocking mode. It has been shown that for a perfect orthorhombic structure the integrated intensities of the two components of the split scissoring mode are equal if unpolarized radiation is used for sampling. For polarized radiation the integrated intensities of the two components will be equal if the subcell is oriented 45° with respect to the *x*,*y* axis. Therefore, it is possible to calculate the orientation of the subcell in the *x*,*y* plane for a particular experiment, by evaluating the component intensities of the split band for p- or s-polarized radiation.

In Figure 12 the split methylene scissors band is inverted and displayed for p- and s-polarization for a particular experiment on a D_2O subphase. It is found that the relative intensities of the two components switch when the direction of the polarization is reversed. To determine the relative peak areas, the peaks were fit with standard software (Figure 12). The ratio of I_p^{1472}/I_p^{1462} is found to be 1.32, while for I_s^{1462}/I_s^{1472} a value of 1.38 is found; i.e., within the limits of error the ratios are indeed reversed for the two polarizations. This proves that the two molecules in the subcell are indeed orthogonal to each other. For a Cartesian coordinate system, the *z* axis was chosen normal to the interface, while the *x* axis is located so that the plane of incidence is the *x*,*z* plane (Figure 7). The electric vector in p-polarization thus has *x* and *z* components. However, since the molecule was found to be untilted and the transition moment of the scissor mode makes an angle of 90° with the molecule axis, the *z* component will be zero. The *y* axis is the direction of the electric vector in s-polarization. Therefore, the orientation of the subcell in the plane can be easily calculated on the basis of either the p- or s-polarized measurement. For example, the angle that the *a* direction of the subcell makes with the *y* axis {arccot(I_s 1472/I_s 1462)} was found to be 36° for the particular experiment described above.

Acknowledgment. This work was supported by the U.S. Public Health Service through Grant GM 29864 to R.M. Additional funds for spectrometer construction were provided by Rutgers University. A.G. was supported by a grant from the Deutsche Forschungsgemeinschaft (DFG).

Appendix A

A coefficient of reflection, $\tilde{r}$, at an interface between two semi-infinite, homogeneous isotropic phases, where the incident phase (e.g., air) is nonabsorbing and the final phase (e.g., water) is absorbing, is defined as the electric field intensity ratio of the reflected ray to the incident ray. For s- and p-polarization, $\tilde{r}_s$ and $\tilde{r}_p$ can be calculated from the Fresnel equations.

For s-polarization

$$\tilde{r}_s^{\,F} = \sin(\varphi_1 - \tilde{\varphi}_2)/\sin(\varphi_1 + \tilde{\varphi}_2)$$

and for p-polarization

$$\tilde{r}_p^{\,F} = \tan(\varphi_1 - \tilde{\varphi}_2)/\tan(\varphi_1 + \tilde{\varphi}_2)$$

φ_1 is the angle between the incoming ray and the direction of the surface normal, $\tilde{\varphi}_2$ is the complex angle of the refracted ray, and superscript F denotes a Fresnel, i.e., film-free surface (see Figure 7). The respective reflection coefficients for a thin anisotropic film between two semiinfinite phases can be calculated as follows:

$$\tilde{r}_s = -\{\sin(\varphi_1 - \tilde{\varphi}_2) - ik_0\tilde{n}_2^{-1}\sin\varphi_1\tilde{I}_1\}/\{\sin(\varphi_1 + \tilde{\varphi}_2) - ik_0 n_2^{-1}\sin\varphi_1\tilde{I}_1\}$$

$$\tilde{r}_p = \{\sin(\varphi_1 - \tilde{\varphi}_2)\cos(\varphi_1 + \tilde{\varphi}_2) - ik_0\tilde{n}_2^{-1}\sin\varphi_1(\tilde{I}_1\cos\varphi_1\cos\tilde{\varphi}_2 - \tilde{I}_2\sin\varphi_1\sin\tilde{\varphi}_2)\}/\{\sin(\varphi_1 + \tilde{\varphi}_2)\cos(\varphi_1 - \tilde{\varphi}_2) - ik_0\tilde{n}_2^{-1}\sin\varphi_1(\tilde{I}_1\cos\varphi_1\cos\tilde{\varphi}_2 + \tilde{I}_2\sin\varphi_1\sin\tilde{\varphi}_2)\}$$

where $k_o = 2\pi/\lambda$; $\tilde{n}_2$ is the complex refractive index of water; and

$$\tilde{I}_1 = (\tilde{n}_x^{\,2} - \tilde{n}_2^{\,2})d \qquad \tilde{I}_2 = (\tilde{n}_z^{\,2} - \tilde{n}_2^{\,2})d/\tilde{n}_z^{\,2}$$

$\tilde{n}_x$ and $\tilde{n}_z$ are the complex directional refractive indices of the surface layer, while *d* is its thickness. The reflectivity of the film-free and film-covered surface can be calculated by multiplying the respective reflection coefficient with its complex conjugate:

$$R_j = \tilde{r}_j\tilde{r}_j^{\,*}$$

and the reflectance−absorbances RA are obtained as follows:

$$RA_j = -\log(R_j/R_j^{\,F})$$

where *j* denotes s- or p-polarization.

Appendix B

To calculate the directional imaginary parts of the surface layer refractive index, k_x and k_z, Fraser and MacRae's equations[21] for uniaxial films are used, i.e.,

$$k_{x\max} = \{f(\sin^2 \alpha)/2 + (1 - f)/3\}k_{\max}$$

$$k_{z\max} = \{f(\cos^2 \alpha) + (1 - f)/3\}k_{\max}$$

where $f = (3 \cos^2\theta - 1)/2$ and $k_{\max}$ is the dipole moment strength.

To simulate an entire band, a line shape such as a Lorentzian or Gaussian distribution is assumed for the wavenumber dependence of the respective film extinction coefficients and the corresponding anomalous dispersion curve for the film refractive indices, e.g. (Lorentzian case),

$$k_x(\nu) = k_{x\max}\gamma^2/(4\Delta^2 + \gamma^2), \quad k_z(\nu) = k_{z\max}\gamma^2/(4\Delta^2 + \gamma^2)$$

$$n_x(\nu) = n_{\max} - 2\Delta k_{x\max}\gamma/(4\Delta^2 + \gamma^2)$$

$$n_z(\nu) = n_{\max} - 2\Delta k_{z\max}\gamma/(4\Delta^2 + \gamma^2)$$

where $\gamma = 2\pi c(\text{fwhh})$, $\Delta = 2\pi c(\nu - \nu_0)$, fwhh is the full width at half-height, c is the speed of light, ν_0 is the center frequency, and ν is the frequency for which the calculation is being made. The complex refractive indices in the x and z directions, $\tilde{n}(\nu) = n(\nu) + ik(\nu)$, are obtained by combining appropriately the above parameters. The real part of the refractive index, n, is assumed to be isotropic (see text). However, it can be easily separated into its components.

References and Notes

(1) McConnell, H. M. *Annu. Rev. Phys. Chem.* **1991**, *42*, 171. Stine, K. J. *Microsc. Res. Tech.* **1994**, *27*, 439.

(2) Vollhardt, D. *Adv. Colloid Interface Sci.* **1996**, *64*, 143.

(3) Als-Nielsen, J.; Kjaer, K. In *Phase Transition in Soft and Condensed Matter*; Riste, T., Sherrington, D., Eds.; NATO Ser. B, Vol. 211; Plenum Press: New York, 1989; pp 251−321. Als-Nielsen, J.; Möhwald, H. In *Handbook on Synchroton Radiation*; Ebashi, S., Koch, M., Rubenstein, E., Eds.; Elsevier/North-Holland: Amsterdam, 1991; pp 1−53. Als-Nielsen, J.; Jacquemain, D.; Kjaer, K.; Lahav, M.; Leveiller, F.; Leiserowitz, L. *Phys. Rep.* **1994**, *246*, 251.

(4) Mendelsohn, R.; Brauner, J. W.; Gericke, A. *Annu. Rev. Phys. Chem.* **1995**, *46*, 305.

(5) Dluhy, R. A.; Stephens, S. M.;Widayati, S.; Williams, A. D. *Spectrochim. Acta, Part A* **1995**, *51*, 1413.

(6) Vaknin, D.; Kjaer, K.; Nielsen, J. A.; Lösche, M. *Biophys. J.* **1991**, *59*, 1325. Brezesinski, G.; Dietrich, A.; Struth, B.; Böhm, C.; Bouwman, W. G.; Kjaer, K.; Möhwald, H. *Chem. Phys. Lipids* **1995**, *76*, 145. Baltes, H.; Schwendler, M.; Helm, C. A.; Möhwald, H. *J. Colloid Interface. Sci.* **1996**, *178*, 135.

(7) Hosoi, K.; Ishikawa, T.; Tomioka, A.; Miyano, K. *Jpn. J. Appl. Phys.* **1993**, *32*, 135. Weidemann, G.; Vollhardt, D. *Thin Solid Films* **1995**, *264*, 94.

(8) Dluhy, R. A. *J. Phys. Chem.* **1986**, *90*, 1373. Fina, L. J.; Tung, Y. S. *Appl. Spectrosc.* **1991**, *45*, 986. Gericke, A.; Michailov, A. V.; Hühnerfuss, H. *Vib. Spectrosc.* **1993**, *4*, 335. Tung, Y. S.; Gao, T.; Rosen, M. J.; Valentini, J. E.; Fina, L. J. *Appl. Spectrosc.* **1993**, *47*, 1643. Ren, Y.; Meuse, C. W.; Hsu, S. L.; Stidham, H. D. *J. Phys. Chem.* **1994**, *98*, 8424. Blaudez, D.; Turlet, J.-M.; Dufourcq,J.; Bard, D.; Buffeteau, T.; Desbat, B. *J. Chem. Soc., Faraday Trans.* **1996**, *92*, 525.

(9) Flach, C. R.; Brauner, J. W.; Mendelsohn, R. *Biophys. J.* **1993**, *65*, 1994. Pastrana-Rios, B.; Taneva, S.; Keough, K. M. W.; Mautone, A. J.; Mendelsohn, R. *Biophys. J.* **1995**, *69*, 2531. Flach, C. R.; Prendergast, F. G.; Mendelsohn, R. *Biophys. J.* **1996**, *70*, 539. Cornut, I.; Desbat, B.; Turlet, J.-M.; Dufourcq, J. *Biophys. J.* **1996**, *70*, 305.

(10) Gericke, A.; Hühnerfuss, H. *Ber. Bunsen-Ges. Phys. Chem.* ***1995***, 99, 641.

(11) Gericke, A.; Hühnerfuss, H. *J. Phys. Chem.* **1993**, *97*, 12899.

(12) Mendelsohn, R.; Snyder, R. G. In *Biological Membranes*; Merz, K. M., Roux, B., Eds.; Birkhäuser: Boston, 1996; pp 145−174. Snyder, R. G. *J. Chem. Phys.* **1979,** *71***,** 3229.

(13) Snyder, R. G.; Liang, G. L.; Strauss, H. L.; Mendelsohn, R. *Biophys. J.* in press.

(14) Flach, C. R.; Brauner, J. W.; Taylor, J. W.; Baldwin, R. C.; Mendelsohn, R. *Biophys. J.* **1994**, *67*, 402. Blaudez, D.; Buffeteau, T.; Cornut, J. C.; Desbat, B.; Escarfre, N.; Pezolet, M.; Turlet, J. M. *Appl. Spectrosc.* **1993**, *47*, 869.

(15) Schopper, H. *Z. Phys.* **1952**, *132*, 146.

(16) Kuzmin, V. L.; Michailov, A. V. *Opt. Spectrosc.* **1981**, *51*, 383. Kuzmin, V. L.; Romanov, V. P.; Michailov, A. V. *Opt. Spectrosc.* **1992**, *73*, 3.

(17) Yamamato, K.; Ishida, H. *Appl. Spectrosc.* **1994**, *48*, 775.

(18) Röseler, A.; Dietel, R.; Korte, E. H., submitted for publication.

(19) Röseler, A.; Gericke, A.; Korte, E. H.; Mendelsohn, R., to be published.

(20) Tanford, C *J. Phys. Chem.* **1972**, *76*, 3020.

(21) Fraser, R. D. B.; MacRae, T. P. *Conformation in Fibrous Proteins and Related Synthetic Polypeptides*; Academic Press: New York, 1973.

(22) Cameron, D. G.; Casal, H. L.; Mantsch, H. H. *Biochemistry* **1980**, *19*, 3665.

(23) Ulman, A. *Ultrathin Organic Films*, Academic Press, Boston, 1991.

(24) Gutberlet, T.; Vollhardt, D. *J. Colloid Interface Sci.* **1995**, *173*, 429.

(25) Buontempo, J. T.; Rice, S. A. *J. Chem. Phys.* **1993**, *98*, 5825.

(26) Yamamoto, K.; Ishida, H. *Vib. Spectrosc.* **1994**, *8*, 1.

(27) Snyder, R. G. *J. Mol. Spectrosc.* **1960**, *4*, 414. Snyder, R. G. *J. Mol. Spectrosc.* **1961**, *7*, 116.

(28) Bertie, J. E.; Ahmed, M. K.; Eysel, H. H. *J. Phys. Chem.* **1989**, *93*, 2210.